Asia Pacific Academy of Science Pte. Ltd.

Computer and Telecommunication Engineering 2024, 2(2), 2452.
https://doi.org/10.54517/cte.v2i2.2452

Article

Semi-autonomous sensor fusion-based strategy for unmanned aerial atmospheric surveillance system in open field environments

Yassen Gorbounov[1,2,*], Zahari Dinchev[3], Petar Peychinov[1]

[1] Department of Automation of Production Systems, University of Mining and Geology, Sofia 1700, Bulgaria
[2] Department of Informatics, New Bulgarian University, Sofia 1618, Bulgaria
[3] Department of Mine Ventilation and Technical Safety, University of Mining and Geology, Sofia 1700, Bulgaria
*** Corresponding author:** Yassen Gorbounov, y.gorbounov@mgu.bg

CITATION

Gorbounov Y, Dinchev Z, Peychinov P. Semi-autonomous sensor fusion-based strategy for unmanned aerial atmospheric surveillance system in open field environments. Computer and Telecommunication Engineering. 2024; 2(2): 2452. https://doi.org/10.54517/cte.v2i2.2452

ARTICLE INFO

Received: 29 December 2023
Accepted: 14 June 2024
Available online: 18 July 2024

Abstract: This paper explores the convergence of semi-autonomous systems and sensor fusion for monitoring hazardous atmospheric substances in open and semi-confined environments such as open-pit mines. As the heart of this system, a universal and flexible device leveraging wireless technologies to collect and analyze large volumes of data, designed by the authors, is proposed. The article outlines the key components of the platform, emphasizing its potential for increasing personnel safety levels as stipulated by the international public exposure guidelines. In modern mines, it becomes crucial to monitor elevated concentrations of nitrogen and carbon oxides, as well as other pollutants after blasting and the toxic gas emissions produced by the heavy transportation equipment such as mining trucks and excavators. In this paper, industrial-grade electrochemical sensors are compared with price-affordable but less precise microelectrochemical ones. The performed experiments for lowering computational requirements show promising results. The integration of an ultrasonic anemometer enhances the system's capabilities, contributing to a comprehensive understanding of atmospheric conditions. In parallel, the research discusses the role of computer vision in autonomous control systems, with a focus on the architecture and processing pipeline of the state-of-the-art system-on-module Kria by AMD. Advocating the potential of adaptive computing for enhanced efficiency in dynamic environments, the paper underlines the importance of the integrated approach in developing a semi-autonomous atmospheric surveillance system and highlights the impact of adaptive computing in dynamic scenarios. The main part of the measuring equipment and methods has been experimented with in real conditions in open-pit mines in Bulgaria. This is an initial phase of ongoing research aimed at serving as a foundation for future improvements and the elaboration of a fully autonomous prototype for hazardous substances evaluation in the atmosphere of open-pit mines.

Keywords: IoT; wireless network; gas sensor; autonomous systems; atmospheric surveillance; technical safety

1. Introduction

Modern mineral extraction processes are inconceivable without the deployment of explosives, characterized by their cost-effectiveness and capacity to liberate substantial energy rapidly harnessed for rock crushing applications. In the context of opencast mining, the utilization of explosives results in the emission of numerous toxic gases, directly infiltrating the open-pit mine's atmosphere, thereby posing a tangible hazard to workers. The initial cloud characterization after blasting can be seen in **Figure 1a**, and the ensuing hazardous gas distribution is given in **Figure 1b**. Beyond the harmful effects of explosive detonations, which introduce elevated concentrations of nitrogen and carbon oxides into the work environment, the internal combustion

engines of mining trucks and excavators further compromise the open-pit mine atmosphere. These engines combust significant quantities of diesel fuel, contributing to atmospheric pollution. The spectrum of pollution sources encompasses dust, gases, noise, and even radioactive compounds [1–4]. The detrimental gases discharged during blasting primarily include nitrogen oxide (NO), nitrogen dioxide (NO_2), carbon monoxide (CO), and sulfur dioxide (SO_2), with potential variations depending on the chemical composition of the rocks and explosives employed.

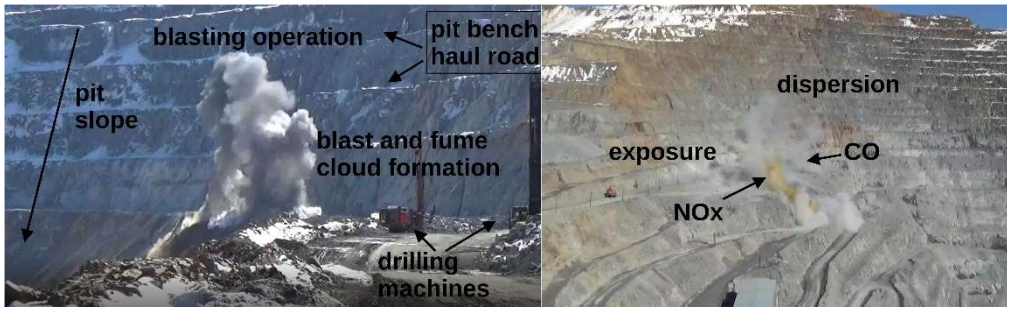

(a) **(b)**

Figure 1. The scientific perspective of the initial cloud characterization. **(a)** blasting operation; **(b)** gas distribution after the explosion.

Explosives, despite their cost-effectiveness and inherent safety, pose a heightened risk of generating a concentrated toxic milieu in the event of a "volley" explosion. The NO and NO_2 are often found as by-products in the post-blast gases of ammonium nitrate-based (NH_4NO_3) explosives. Together, these gases are referred to as "NO_x". While nitric oxide is imperceptible, nitrogen dioxide manifests in hues ranging from yellow to dark red, contingent upon the concentration and dimensions of the gas cloud.

The American Industrial Hygiene Association (AIHA) [5] has established international public exposure guidelines, including the Emergency Response Planning Guidelines (ERPG), which delineate three tiers of exposure values. Furthermore, Immediate Danger for Life and Health (IDLH) [6] specifies the maximum allowable exposure level to a given hazard for a healthy individual over a 30-minute duration, beyond which irreversible health consequences may occur.

Table 1 provides the permissible concentrations for an 8 h total weight average (TWA) permissible exposure limit (PEL) and short-term exposure limit (STEL) concentration, allowing exposure for up to 15 min.

Table 1. Permissible concentrations for toxic gases.

Toxic gas	Concentration, ppm [5]			
	IDLH [7] (≤ 30 min)	ERPG-3 (≤60 min)	TWA	STEL
NO_2	13	20	0.5	1
NO	100	-	2	-
SO_2	100	25	0.5	1
CO	1200	500	20	100

A medium-sized open-pit mine utilizes varying quantities of explosives weekly,

ranging from several dozen to several hundred tons, with detonations occurring once or twice. Each kilogram of explosive yields an average of 110 L of NOx. Simultaneous detonations in multiple blast fields, located at different elevations within the mine, are common. Post-blast, ensuring safe working atmosphere necessitates diluting toxic gases to prescribed levels. Large open-pit mines rely on natural ventilation, contingent on mine configuration and atmospheric conditions during blasting, including wind speed, direction, temperature, air pressure, sunlight, and humidity. Natural ventilation duration, influenced by diverse atmospheric conditions, ranges from minutes to days, especially in the presence of temperature inversions and wind absence. Portable devices, carried by workers overseeing blasting operations, are employed to measure gas content post-blast. Workers must inspect blast fields for potential failed charges and assess toxic gas concentrations before granting permission for other mineworkers to resume activities. The mine's intricate aerodynamics can create "recirculation" zones, elevating toxic gas concentrations to dangerous levels. Therefore, monitoring cloud size, gas concentration, and downstream dispersion is crucial to enhance downtime efficiency and bolster safety measures.

Presently, prevalent in use are wearable portable gas detectors worn by personnel, specifically designed for monitoring gas concentration levels within excavation zones [8]. However, these detectors lack the capacity to capture data for in-depth and thorough analysis. In addition, this method of surveying hazardous areas still requires human intervention, which poses serious health risks. **Figure 2** displays certain widely adopted portable detectors utilized in mining, with their functionalities summarized in **Table 2**.

(a) **(b)** **(c)** **(d)** **(e)** **(f)**

Figure 2. Popular wearable gas detectors used in mining (models disclosed in **Table 2**).

Table 2. Characteristics of portable gas detectors from **Figure 2**.

Figure 2	Type	Model	Gas (range, resolution)	Price [EUR]
(a)	single gas	Drager PAC5500	CO (0–500 ppm, 1 ppm), H_2S (0–100 ppm, 0.1 ppm), O_2 (0–25 vol%, 0.1 vol%)	650
(b)	single gas	Industrial Scientific Tango TX1	CO (0–1000 ppm, 1 ppm), H_2S (0–500 ppm, 0.1 ppm), SO_2 (0–150 ppm, 0.1 ppm), NO_2 (0–150 ppm, 0.1 ppm)	400
(c)	single gas	Industrial Scientific Gasbadge Pro	CO (0–1500 ppm, 1 ppm), H_2S (0–500 ppm, 0.1 ppm), SO_2 (0–150 ppm, 0.1 ppm), O_2 (0–30 vol%, 0.1 vol%), NO_2 (0–150 ppm, 0.1 ppm), NH_3 (0–500 ppm, 1 ppm), CL_2 (0–100 ppm, 0.1 ppm), CLO_2 (0–1 ppm, 0.01 ppm), PH_3 (0–10 ppm, 0.01 ppm), HCN (0–30 ppm, 0.1 ppm), H_2 (0–2000 ppm, 1 ppm)	640
(d)	multigas	MSA Altair 4X Mining	CH_4 (0–5%, 0.05%), O_2 (0–30 vol%, 0.1 vol%), CO (0–1999 ppm, 1 ppm), NO_2 (0–50 ppm, 0.1 ppm), H2S (0–200 ppm, 1 ppm)	1600

Table 2. (*Continued*).

Figure 2	Type	Model	Gas (range, resolution)	Price [EUR]
(e)	multigas	Honeywell BW Max XT II	LEL (0–100%, 1%), O_2 (0–30 vol%, 0.1 vol%), CO (0–1000 ppm, 1 ppm), H_2S (0–200 ppm, 1 ppm)	1200
(f)	multigas	Drager X-am 5600	CO_2 (0–5 vol%, 0.1 vol%), O_2 (0–25 vol%, 0.1 vol%), CO (0–2000 ppm, 2 ppm), H_2S (0–200 ppm, 1 ppm)	2000

Reducing human factor, increasing safety, and automating production is a hot topic and a serious challenge in the mining industry. Nowadays, the technological level has reached the fourth industrial revolution (Industry 4.0), which includes mechatronics, the Internet of Things (IoT), and artificial intelligence (AI). That paves the way for the introduction of autonomous systems in mining [9]. The levels assigned to mining equipment are based on the Society of Automotive Engineers (SAE) taxonomy [10] of driving automation terms and adapted to apply to mining automation using the ISO 17757:2017 standard. There exist six levels of autonomy that are summarized in **Figure 3** ([10] with additions).

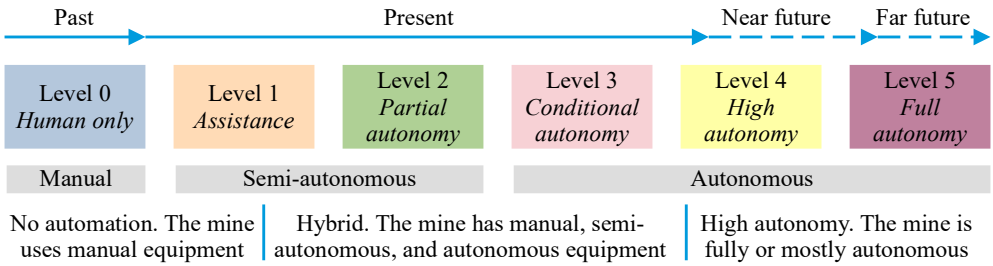

Figure 3. The six levels of autonomy.

The main objective of this work, as described above, is to develop a semi-autonomous system for atmospheric monitoring in an open-pit mine following blasting operations and for evaluating the potential risk of significant structural changes. Some of the modules of the system are built and verified in practice, while others are subject to future work. The proposed system presents the initial stage of ongoing research. It includes a device for measuring toxic gas concentrations, monitoring the direction and dimensions of the wind, a computer vision subsystem, and a communication environment allowing the transfer of the measured data in real time. The system architecture of the proposed platform is given in **Figure 4**.

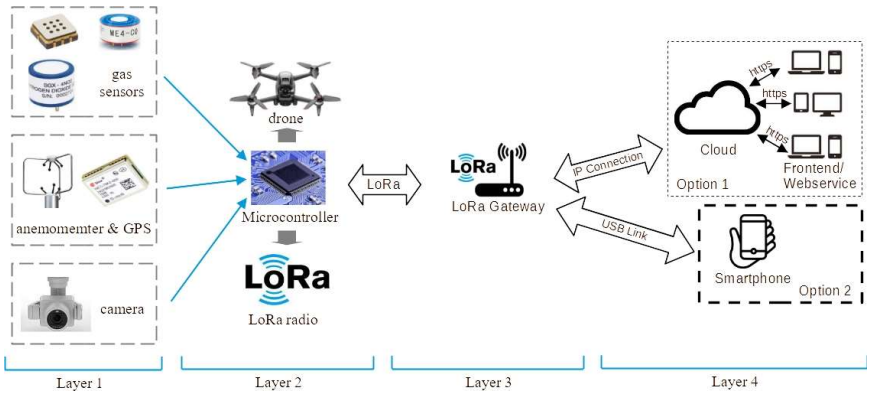

Figure 4. System architecture of the modular mobile monitoring device.

The system consists of four layers. The first layer is sensory and contains the camera, the multi-gas sensing apparatus, and the ultrasonic anemometer, which gives a three-dimensional picture of the wind vector. The second layer includes the unmanned aerial vehicle (UAV) that carries the sensors from layer 1, which are connected to the microcontroller subsystem and can communicate with the third layer using LoRa [11] (long range) physical radio communication technique. The fourth layer provides several options to read, store, and further analyze the collected data. The proposed system architecture provides a portable yet powerful integrated sensor fusion-based strategy for UAV atmospheric surveillance systems that applies in open field environments. A use case scenario employing the above activities is illustrated in **Figure 5a**, and the modules performing data acquisition operations appear in **Figure 5b**. In the same figure, the flow of data collection and processing can be seen. It consists in the simultaneous measurement of key atmospheric parameters, including the spatial wind vector, which, together with the object recognition subsystem, supports the automated repositioning of the UAV and data recording and transmission of the latter to the base station.

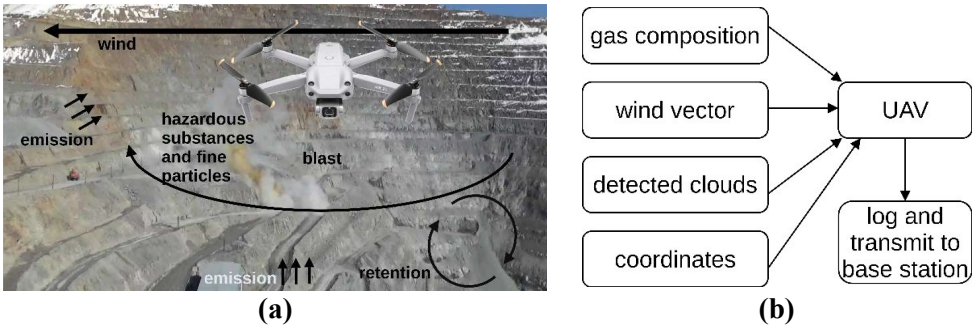

(a) **(b)**

Figure 5. (a) Example of atmosphere monitoring operation in real case situation; **(b)** block diagram of the data acquisition process.

The proposed sensor fusion-based strategy for UAV atmospheric surveillance is capable of performing complex analysis of harmful substances by simultaneously monitoring not only several critical parameters at a time but also predicting their proliferation in real time and estimating the most active zones using object recognition. Semi-autonomous and fully autonomous monitoring systems can replace humans in post-blast gas toxicity monitoring in opencast mines. This is confirmed by many studies [12–16] where the use of UAV is proposed. However, none of these studies included an integrated measurement of the spatial wind vector, which can be key in assessing the mine atmosphere. Undoubtedly, this would improve the productivity of the mining enterprise and reduce the number of accidents. The authors are gradually implementing this novel approach in real-world settings.

The subsequent sections of this paper are structured as follows: Chapter 2 presents a concise comparison of gas detection sensors and proposes the structure of a gas measurement device. Chapter 3 elucidates the operational principles of the 3D ultrasonic anemometer. Chapter 4 gives insights on the computer vision subsystem, while Chapter 5 delineates the communication layer. Chapter 6 offers perspectives on potential enhancements for both the device and methodology. This section concludes the paper.

2. Gas measurement device

Within the realm of existing gas sensor technologies, four principal categories can be identified [17–19], each distinguished by its underlying physical principle: optical sensors, mass sensors, electrochemical sensors, and thermal sensors. Optical sensors operate on the principle of light absorption at varying wavelengths within the spectrum, depending on gas properties—essentially employing spectroscopic methods. While highly selective, they tend to be costly, power-intensive, and voluminous. Mass sensors detect frequency shifts in acoustic waves caused by the absorption of molecules onto an oscillating structure's surface [20]. They consume less power and have very high performance, high sensitivity, and fast response. Electrochemical sensors [21], relying on oxidation-reduction reactions with gas molecules, generate an electrical signal corresponding to gas concentration. These sensors exhibit high sensitivity, linear output, and ease of use. However, they have a limited shelf life, are sensitive to interferents, and may experience shortened lifespans in excessively dry or hot environments. Thermal conductivity-based sensors detect gas by monitoring temperature-induced resistance changes resulting from combustion reactions in catalytic materials. While offering a broad measurement range, these sensors exhibit non-specificity and are cross sensitive to other compounds. They do not function effectively with gases possessing thermal conductivities close to one (e.g., air, NH_3, CO, NO, O_2, N_2), and measurements become challenging when dealing with thermal conductivities less than one. Despite producing a non-linear output signal, these sensors are cost-effective and reliable in dusty environments. In this study, the proposed platform accommodates electrochemical and microelectromechanical (MEMS) sensors. The fundamental structure of electrochemical sensors is depicted in **Figure 6a**, and the working principle of the MEMS sensors is given in **Figure 6b**.

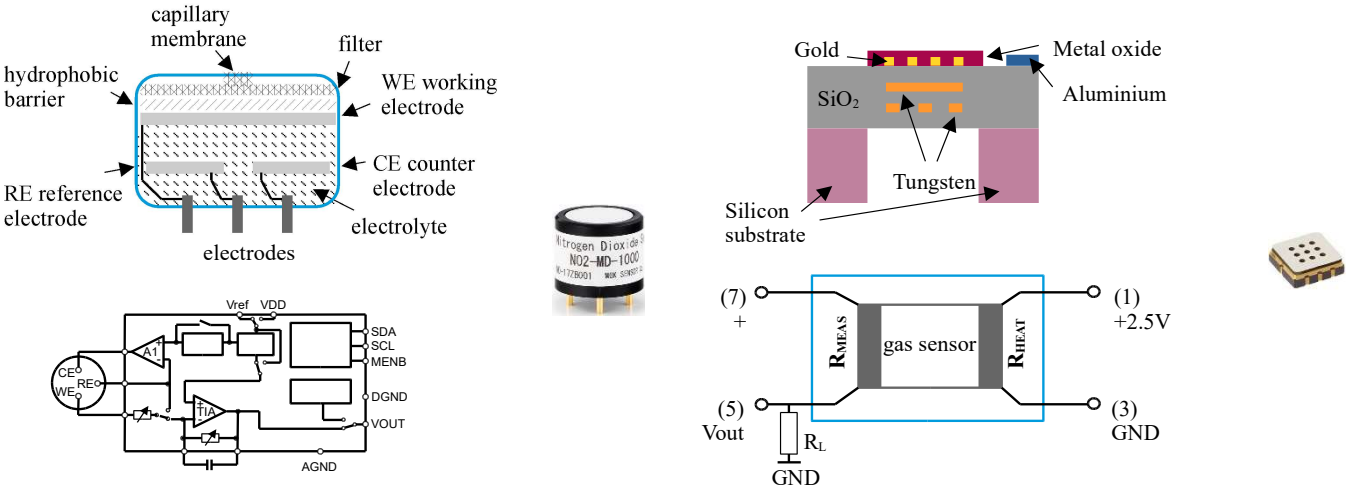

(a) **(b)**

Figure 6. Basic structure, connection diagram and physical view of the electrochemical. **(a)** MEMS; **(b)** sensors.

The electrochemical sensor consists of a working electrode (WE), a counter electrode (CE), and a thin layer of electrolyte between them. In case an external driving voltage is required, there is a reference electrode (RE). Different sensors have different

types of selective membranes, electrolytes, and working electrode types depending on the specific kind of ambient gas. Due to their high price, limited lifetime, and the influence of the wind velocity on the chemical equilibrium in the sensor and thus the influence on the reading correctness [22], in the current study the physical experiment uses MEMS sensors. They are mass sensors based on a micro-hotplate. These sensors possess significant measurement stability and are more suitable for qualitative rather than quantitative measurements.

From an electrical point of view, such a sensor can be seen as a two-resistor device. The R_{HEAT} element has a resistance of about 80 Ohms with very low accuracy ±20%) and acts as a 50 mW heater used to preheat the module before starting the measurement. The R_{MEAS} resistor is the sensitive element. Connecting it in a voltage divider configuration allows for measuring the voltage drop across the load resistor R_L and then obtaining a digital code with the aid of an analog to digital converter (ADC). The results from the experiments are given in **Figure 7.** They represent the verified static characteristics of two sensors—the Winsen GM-102B for the NO gas and the Winsen GM-702B for the CO gas.

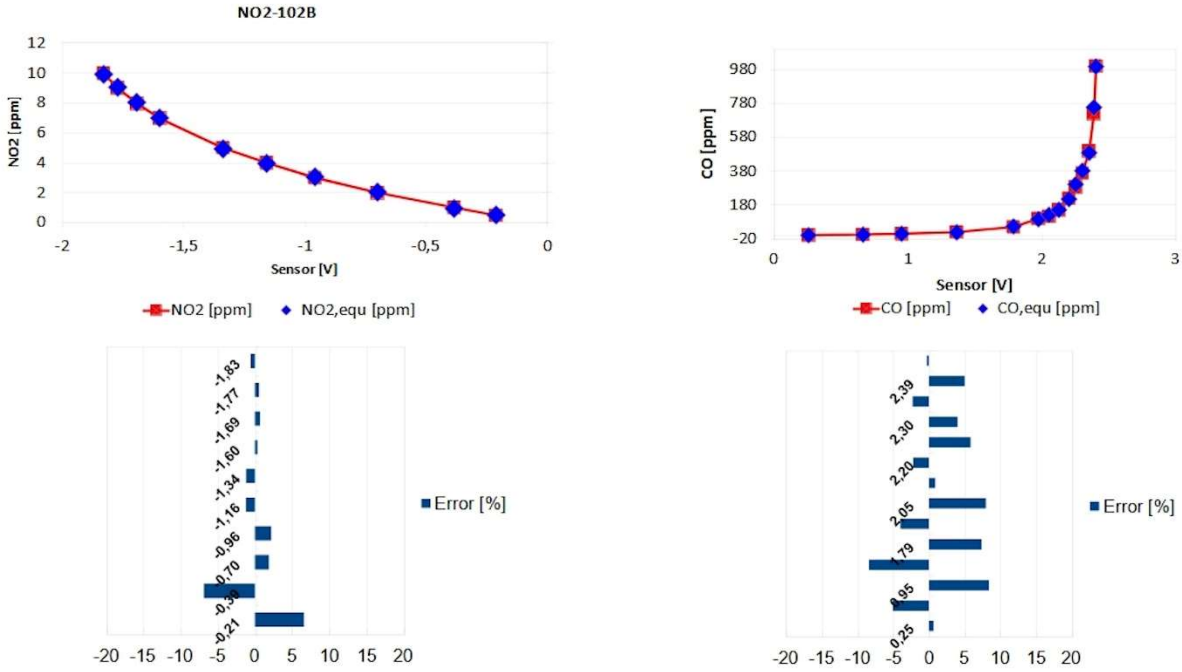

(a) **(b)**

Figure 7. Calibration curves and error plots after the optimized polynomial approximation for the GM-102B (NO_2). **(a)** and the GM-702B (CO); **(b)** MEMS gas sensors.

It is expected that the computation device (the microcontroller part) will run data preprocessing and extensive calculations, so the coefficients in the polynomial approximation of the static characteristics of the gas sensors are presented using fixed-point or integer numbers. This is done by first upscaling these coefficients by a factor that is a power of two and then downscaling the final result by the same factor. The up- and downscaling can be easily implemented with the aid of left-shift and right-shift operations, which are quite fast. The static characteristic for the CO sensor (GM-702) is described in two sub-ranges using two polynomials. In the range 0.2V–2.13V

it is given by (1), and in the range 2.13V–2.4V it is given by (2)—see **Table 3**.

Table 3. Polynomial equations and their coefficients.

No	Equation	Sensor	Coefficients
(1)	$y = a + b.x + c.x^2 + d.x^3 + e.x^4$	CO—range 1	a = 17.79251, b = –121.72370, c = 269.72562, d = –214.64894, e = 60.53236
		NO_2	a = 0.38848, b = 0.82322, c = 8.12469, d = 6.62335, e = 2.17539
(2)	$y = a + b.x + c.x^2 + d.x^3 + e.x^4 + f.x^5 + g.x^6$	CO—range 2	a = 1176266431, b = –3259312339, c = 3760050587, d = –2311641410, e = 798788991.2, f = –147098079.5, g = 11278154.95

For the CO sensor, the scaling factor is 1024 in range 1 and it is 2 in range 2. The curve description for the NO_2 sensor is given by the 4-th order polynomial (1) and has a single range with a scaling factor of 1024. Approximating the high-order polynomial with fractional coefficients by using integer coefficients leads to a negligible error—for the nitrogen dioxide it is in the range of –6.8% to 6.6%, and for the carbon monoxide it is in the range of –8.4% to 0.7%. Moreover, if zeroing the highest power coefficients, the error remains in the same range after the scaling procedure, which allows further improving the computational efficiency.

The system architecture of the independent gas sensing and data logging submodule is given in **Figure 8**.

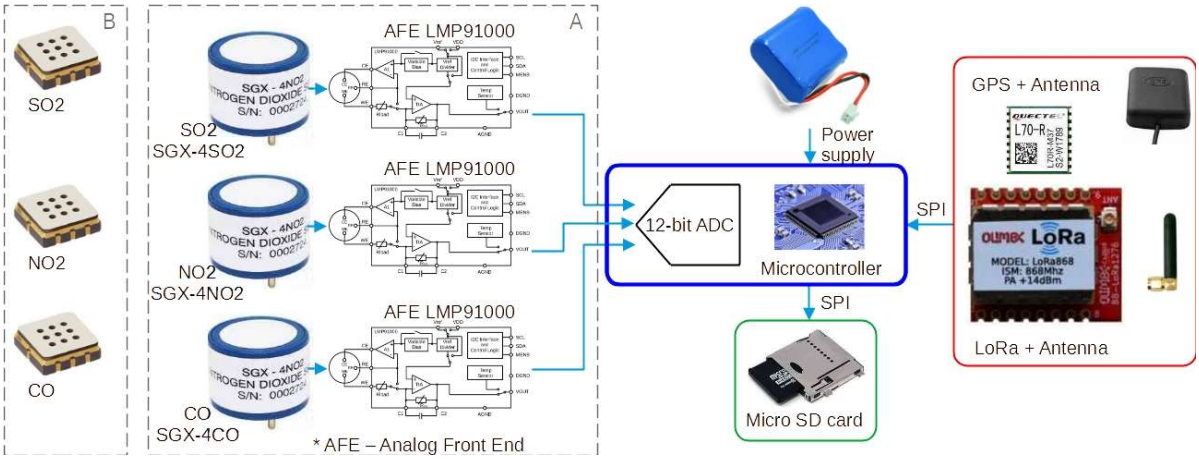

Figure 8. Basic system architecture of the independent gas sensing and data logging device.

The design of the prototype obeys the ideas of modularity, power efficiency, extendibility, and reliability. It is designed to be lightweight and have high computational capabilities. At present, its core is built around the RP2040 microcontroller (MCU) that has a dual-core Arm Cortex-M0+ processor with 264 kB of internal RAM and supports up to 16 MB of off-chip flash. Adding more sensors, such as anemometers, computer vision, and data analytics capabilities, presumes a higher computational power would be required. So attempts are made to substitute the RP2040 MCU with the more powerful K26 SoM that features an ARM Cortex-A53 Quad-Core application and Cortex-R5F Dual-Core real-time processing units along with other high-performance hardware. The LoRa connectivity supports the AES-128 advanced encryption standard. The gas sensing can be done either with the aid of

electrochemical sensors (option A) or MEMS sensors (option B). The first option requires signal conditioning, implemented with the aid of the LMP91000 configurable potentiostat, which is made for low-power electrochemical cells. The measured gas quantities are filtered and calculated before being stored on a micro SD card and transmitting over the LoRa channel. The accurate position of the UAV is captured by the GPS and transmitted along with the data. This is especially useful for simultaneous localization and mapping (SLAM) algorithms and may help in case of lack of visibility. The second option consists of replacing the Analog Font End (AFE) and the electrochemical sensors with MEMS sensors. This solution has been experimented here because it helps in lowering the price and weight, reducing the overall complexity, and increasing the durability of the device.

3. Wind measurement device

A significant part of the working areas in mining present large volumes, and in such areas one-dimensional, directed air currents are rarely observed. Often the currents are of relatively equal magnitude in the three dimensions (x, y, and z). This is how hazardous gases spread in the studied areas. Local air quality and, accordingly, the dangerous concentration of toxic gases and mechanical harm can vary dynamically depending on climatic conditions. For example, the wind rose influences the direction of the toxic vapors (**Figure 9a**).

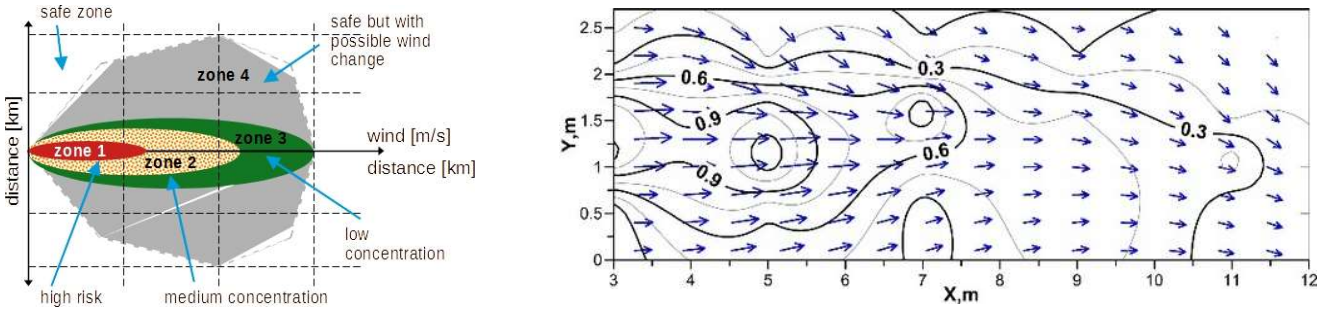

Figure 9. (a) Predicted pollutant concentrations in dependence from the wind direction; **(b)** real measurement made with the aid of the 3D ultrasonic anemometer.

The picture in **Figure 9a** can be modeled with software tools like ALOHA (part of the Computer-Aided Management of Emergency Operations (CAMEO)), TOXI + Risk [23], and other tools. The initial conditions of the simulation can be obtained easily if data on the airflow parameters are available. It can be seen from the figure that in "zone 1" the concentration is extremely high so that the exposure time should be restricted to a minimum, "zone 2" corresponds to medium concentration, and in "zone 3" the amount of toxic gases is relatively low. The relative boundaries of "zone 4" surround an area where the wind can change its direction. It can be observed that moving away from the place of the blast demands time, which can be critical for the moving of mineworkers. Measurements and visualization of the spatial vector field of airflow in free and semi-confined space are possible with a 3D ultrasonic anemometer. This allows the construction of an actual velocity field by rapid multiple measurements in all three directions. A real measurement made with the aid of the 3D ultrasonic

anemometer that shows the XY velocity vectors and lines of equal velocities for a given elevation is shown in **Figure 9b**. An experiment has been conducted using the Young 3D ultrasonic anemometer model 81000 [24–26]. Since it lacks communication capabilities, a modification has been made as depicted in **Figure 10**.

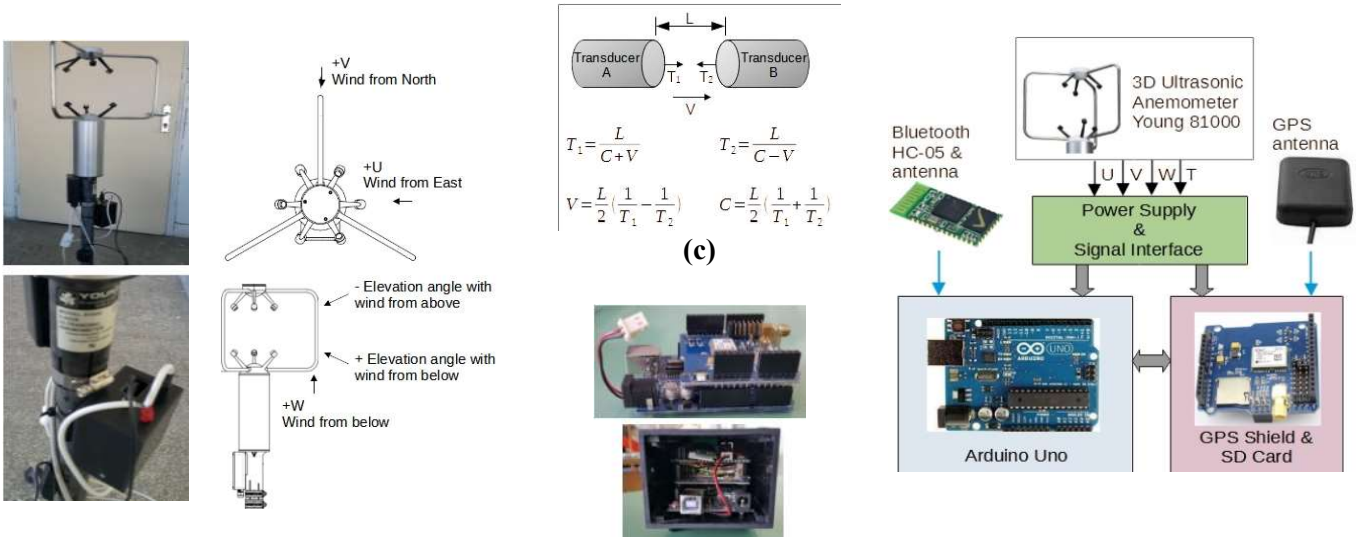

(a) **(b)** **(c)** **(d)** **(e)**

Figure 10. The 3D ultrasonic anemometer prototype. **(a)** the physical device; **(b)** side view and orientation of the anemometer device; **(c)** the time of flight (ToF) principle (C—speed of sound, V—fluid velocity, T1, T2—ultrasound propagation times, L—distance between opposite transducers); **(d)** the implemented device; **(e)** block diagram of the main components.

Ideally, the anemometer must face the north geomagnetic pole or a position that is along the tube. Next, device synchronization is performed, and measurements can be initiated. A comma-separated (CSV) file is created for every measurement cycle, and the data is saved every second. The provided information includes the latitude (GPS_LAT [deg]), the longitude (GPS_LON [deg]), the GPS date (GPS_DATE [dd/mm/yyyy]) and time (GPS_UTC_TIME [UTC hh:mm:ss]), the velocity vector in [m/s] for the three directions, namely U (east/west), V (north/south), and W (down/up), and the temperature of the air flow T [°K]. The ultrasonic wind measurement device aids in creating adequate predictions for the proliferation of hazardous substances in the atmosphere of the open-pit mine.

4. Computer vision subsystem

The expanding role of computer vision in autonomous control systems is evident in the growing demand for enhanced sensor performance, faster image processing, and SLAM algorithms [27–29]. Being an initial stage of an ongoing work, the proposed system suggests the substitution of the conventional embedded microcontroller (the RP2040) with a heterogeneous parallel-processing capable system. This would allow embedding the environment perception, processing, prediction, planning, and decision-making stages in a monolithic device carried by a drone. The ultimate goal is to achieve a fully autonomous UAV for hazardous substances monitoring and analysis in open field environments. Such capabilities can be achieved with the aid of the AMD

Zynq UltraScale+ Multi-Processing System on Chip (MPSoC) Kria System on Module (SoM). The high-level model of this chip [29] is given in **Figure 11**.

The platform includes a field-programmable logic (FPGA) layer (PL) and processing (MCU) subsystem (PS). They connect with the Deep Learning Processing Unit (DPU) with the aid of the on-chip communication Advanced eXtensible Interface (AXI) bus. The DPU is a parameterizable computing engine with inherent support for Convolution Neural Networks (CNN) and Deep Neural Networks (DNN). The input data stream is preprocessed at the PL side. Then it feeds the processing system, where the DPU provides accelerator capabilities.

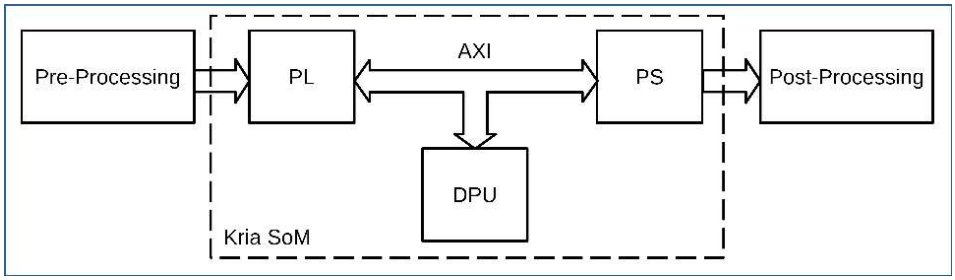

Figure 11. The high-level Kria SoM system.

The block diagram of the DPU [29] is given in **Figure 12**.

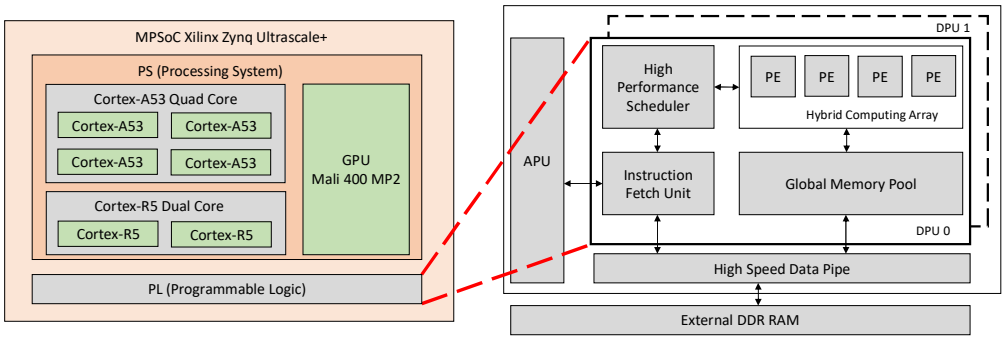

Figure 12. Top-level block diagram of the MPSoC (left) and the DPUCZDX8G (right).

The DPU (DPUCZDX8G) is an Artificial Neural Network (ANN) accelerator built by AMD for their Zynq-series SoC architectures. Based on a configurable PL core connected to the PS subsystem, it allows deploying different NN types that can run in parallel. It includes multiple Programmable Engines (PE) arranged in a hybrid computing array specifically designed for CNN applications. It necessitates instructions for executing NN and accessing input image locations, along with handling temporary data outputs. The Application Processing Unit (APU) is responsible for executing programs that manage interrupts and ensure coherency during data transfers. The business logic operates within the Linux operating system environment, while the accelerator blocks reside in the PL fabric.

(a)

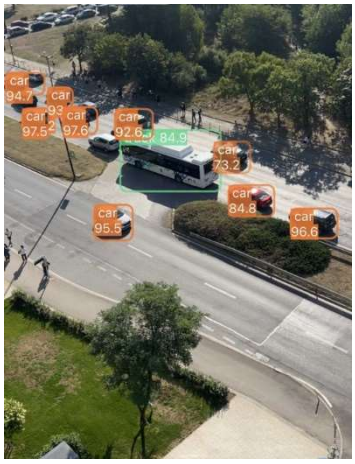

(b)

Algorithm	Platform	Time [s]	CPU Load [%]	RAM [GB]	Frame per sec
SSD	KV260 + accel.	0.15	40	1.6	31
YOLOv8	KV260	1.42	85	1.6	0.63

(c)

Figure 13. Object recognition in a video stream: **(a)**, **(b)** two successive frames; **(c)** algorithm performance comparison.

An object recognition experiment in a video stream has been done with this platform [30]. The results are summarized in **Figure 13**. Two different frames, **Figure 13a** and **Figure 13b**, are shown in the figure. **Figure 13c** compares the performance using two algorithms—the YOLO (You Only Look Once) and the SSD (Single-Shot Detector). The first one runs on the ARM core, while the second one is a video stream accelerator that runs on the PL side. It can be seen that the use of programmable logic outperforms the sequential execution model provided by the microcontroller in terms of processing time and frames per second performance.

5. Communication layer

For effective information exchange within the system, meeting requirements for long-distance data transmission, data protection, and low power consumption is crucial. LoRa wireless communication, a de facto standard in the Internet of Things (IoT) network, fulfills these conditions. LoRa, a trademark of Semtech Corporation, stands for “long range” and is compatible with existing network architectures. It involves a trade-off between data rate and sensitivity within a fixed channel bandwidth, with a range exceeding 10 km. Noteworthy features include a battery life of up to 10 years, cost-effectiveness, robust security via end-to-end AES-128 encryption, and capabilities for firmware updates over the air (FUOTA). LoRa is immune to interference from Wi-Fi, Bluetooth, GSM, LTE, etc. and boasts enhanced network capacity, making it an ideal choice for the proposed atmosphere-monitoring device (**Figure 14**).

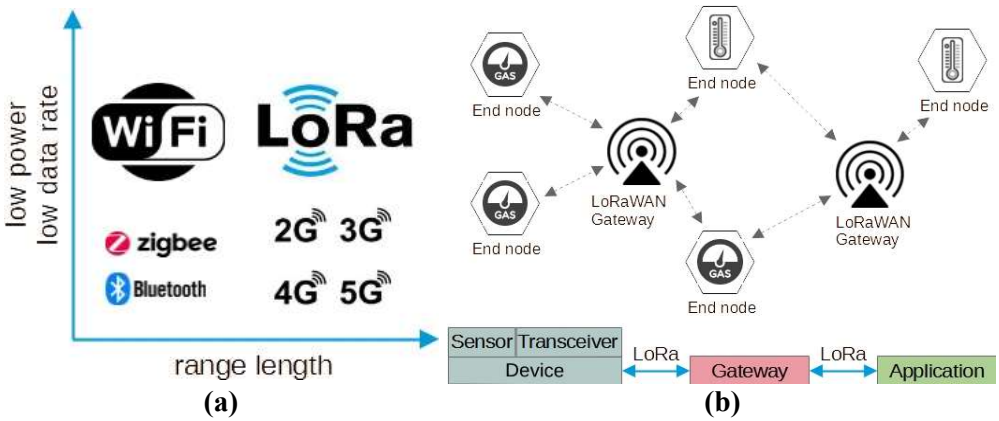

Figure 14. (a) LoRa comparison with other wireless technologies; **(b)** the LoRa topology.

The LoRa network allows flexible topologies such as centralized (star), decentralized (hybrid tree), and distributed (mesh) connections. The protocol allows the continued relay of real-time data in extreme conditions, such as those found in a mine. The above said positions the LoRa network among the best candidates for the mining industry and determines the choice of this wireless technology for the proposed prototype of the semi-autonomous mobile device for monitoring the atmosphere in open-pit mines.

6. Conclusion and future development

The paper outlines the development of a semi-autonomous mine atmosphere monitoring system, introducing and testing essential building blocks such as gas sensors and tools for spatial parameter measurement. This is an initial phase of ongoing research where the modular approach allows for information fusion from various sensors, paving the way for future advancements. Utilizing modern knowledge extraction methods and big data technologies, including artificial neural networks and machine learning, aligns with the modern trends and presents avenues for further exploration. The incorporation of acceleration based on heterogeneous systems, exemplified by the Kria SoM, emerges as a promising strategy to enhance performance and energy efficiency through inherent high parallelism. The study emphasizes the increasing demands for improved sensor performance and accelerated image processing algorithms in autonomous systems. It lays the foundation for future improvements, including the development of a fully autonomous prototype for hazardous substances evaluation in the atmosphere of open-field environments.

Author contributions: Conceptualization, schematics, YG; investigation, ZD; photos, ZD; open-pit data, ZD; computer vision, PP; data acquisition, PP; writing—original draft preparation, YG; writing—review and editing, ZD and PP. All authors have read and agreed to the published version of the manuscript.

Conflict of Interest: The authors declare no conflict of interest.

References

1. Yi H, Zhang X, Yang H, et al. Controlling toxic and harmful gas in blasting with an inhibitor. PLoS ONE. 2023; 18(12): e0291731. doi: 10.1371/journal.pone.0291731
2. Zhang G, Wang E. Risk identification for coal and gas outburst in underground coal mines: A critical review and future directions. Gas Science and Engineering. 2023; 118: 205106. doi: 10.1016/j.jgsce.2023.205106
3. He S, He X, Mitri H, et al. Advances in mining safety theory, technology, and equipment. Advances in Geo-Energy Research. 2023; 10(2): 71-76. doi: 10.46690/ager.2023.11.01
4. Gniewosz M, Stopkowicz A, Cała M. An Analysis of the Impact of Mining Excavation Velocity on the Development of Gaseous and Gaseous Geodynamic Hazards in Copper Ore Mines. Geosciences. 2024; 14(2): 54. doi: 10.3390/geosciences14020054
5. American Industrial Hygiene Association. The AIHA Handbook for ERPG and WEEL. AIHA Press; 2020.
6. National Institute for Occupational Safety and Health. NIOSH Pocket Guide to Chemical Hazards. National Institute for Occupational Safety and Health; 2007.
7. Gerboles M, Buzica D. European Commission. In: Joint Research Centre. Evaluation of Micro-Sensors to Monitor Ozone in Ambient Air. Institute for Environment and Sustainability; 2009. doi: 10.2788/5978
8. Ziętek B, Banasiewicz A, Zimroz R, et al. A Portable Environmental Data-Monitoring System for Air Hazard Evaluation in Deep Underground Mines. Energies. 2020; 13(23): 6331. doi: 10.3390/en13236331
9. Fisher B, Schnittger S. Autonomous and Remote Operation Technologies in the Mining Industry-Benefits and Costs. BAE Research Report; 2012.
10. Global Mining Guidelines Group. Guideline for the Implementation of Autonomous Systems in Mining. Available online: https://gmggroup.org/wp-content/uploads/2019/06/20181008_Implementation_of_Autonomous_Systems-GMG-AM-v01-r01.pdf (accessed on 9 September 2022).
11. Kumar PP, Paul PS, Ananda M. Development of LoRa Communication System for Effective Transmission of Data from Underground Coal Mines. Processes. 2023; 11(6): 1691. doi: 10.3390/pr11061691
12. The DRONESAFE project. Autonomous drones for safer mines. Available online: https://www.ltu.se/research/subjects/RoboticsAI/Forskning/DRONESAFE-1.204090?l=en (accessed on 13 September 2022).
13. Bamford T, Medinac F, Esmaeili K. Continuous Monitoring and Improvement of the Blasting Process in Open Pit Mines Using Unmanned Aerial Vehicle Techniques. Remote Sensing. 2020; 12(17): 2801. doi: 10.3390/rs12172801
14. Ren H, Zhao Y, Xiao W, et al. A review of UAV monitoring in mining areas: Current status and future perspectives. International Journal of Coal Science & Technology. 2019; 6(3): 320–333. doi: 10.1007/s40789-019-00264-5
15. Alvarado M, Gonzalez F, Fletcher A, et al. Towards the Development of a Low Cost Airborne Sensing System to Monitor Dust Particles after Blasting at Open-Pit Mine Sites. Sensors. 2015; 15(8): 19667–19687. doi: 10.3390/s150819667
16. Rossi M, Brunelli D. Autonomous Gas Detection and Mapping with Unmanned Aerial Vehicles. IEEE Transactions on Instrumentation and Measurement. 2016; 65(4): 765–775. doi: 10.1109/tim.2015.2506319
17. Janata J. Principles of Chemical Sensors. Springer US; 2009. doi: 10.1007/b136378
18. Cretescu I, Lutic D, Manea LR. Electrochemical Sensors for Monitoring of Indoor and Outdoor Air Pollution. Electrochemical Sensors Technology. 2017. doi: 10.5772/intechopen.68512
19. Liu H, Zhang L, Li KHH, et al. Microhotplates for Metal Oxide Semiconductor Gas Sensor Applications—Towards the CMOS-MEMS Monolithic Approach. Micromachines. 2018; 9(11): 557. doi: 10.3390/mi9110557
20. Judy JW. Microelectromechanical systems (MEMS): Fabrication, design and applications. Smart Materials and Structures. 2001; 10(6): 1115–1134. doi: 10.1088/0964-1726/10/6/301
21. Ionascu ME, Castell N, Boncalo O, et al. Calibration of CO, NO_2, and O_3 Using Airify: A Low-Cost Sensor Cluster for Air Quality Monitoring. Sensors. 2021; 21(23): 7977. doi: 10.3390/s21237977
22. Poluyan LV, Syutkina EV, Guryev ES. Software Systems for Prediction and Immediate Assessment of Emergency Situations on Municipalities Territories. In: Proceedings of the International Conference on Construction, Architecture and Technosphere Safety (ICCATS 2017); 21-22 September 2017; Chelyabinsk, Russian Federation. doi: 10.1088/1757-899x/262/1/012199
23. Young Company. Ultrasonic Anemometer MODEL 81000. R.M. Young Company; 2017.
24. Dinchev Z, Gorbunov Y. Improvement of Measurements of 3D Air Flows in Free and Semi-Restricted Space. Journal of

Mining and Geological Sciences. 2017; 60: 39-42.
25. Dinchev Z, Gorbunov Y, Kostadinova N. Velocity Field Visualization, Measured with 3D Ultrasonic Anemometer. Journal of Mining and Geological Sciences. 2018; 61: 39-44.
26. Ahmed MF, Masood K, Fremont V, et al. Active SLAM: A Review on Last Decade. Sensors. 2023; 23(19): 8097. doi: 10.3390/s23198097
27. Jia G, Li X, Zhang D, et al. Visual-SLAM Classical Framework and Key Techniques: A Review. Sensors. 2022; 22(12): 4582. doi: 10.3390/s22124582
28. Kalapothas S, Flamis G, Kitsos P. Efficient Edge-AI Application Deployment for FPGAs. Information. 2022; 13(6): 279. doi: 10.3390/info13060279
29. Zynq DPU. Product Guide (PG338). Available online: https://docs.xilinx.com/r/3.2-English/pg338-dpu/Introduction (accessed on 10 January 2023).
30. Gorbounov Y, Peychinov P. Vision and control capabilities of autonomous systems with the Kria Adaptive System-on-Modules. In: Proceedings of the 2023 31st National Conference with International Participation (TELECOM); 16-17 November 2023; Sofia, Bulgaria. pp. 1-4. doi: 10.1109/telecom59629.2023.10409757